

Customizing the Shape and Microenvironment Biochemistry of Biocompatible Macroscopic Plant-Derived Cellulose Scaffolds

Ryan J. Hickey,[†] Daniel J. Modulevsky,[‡] Charles M. Cuerrier,[†] and Andrew E. Pelling^{*,†,‡,§,||}

[†]Centre for Interdisciplinary NanoPhysics, Department of Physics, University of Ottawa, MacDonald Hall, 598 King Edward Ave, Ottawa, ON K1N5N5, Canada

[‡]Department of Biology, University of Ottawa, Gendron Hall, 30 Marie Curie, Ottawa, ON K1N5N5, Canada

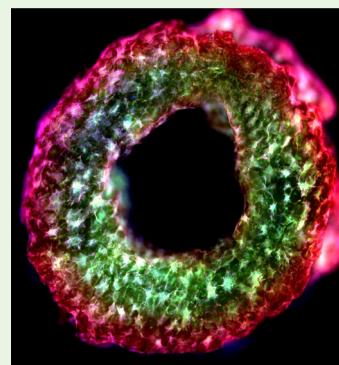
[§]Institute for Science Society and Policy, University of Ottawa, Simard Hall, 60 University, Ottawa, ON K1N5N5, Canada

^{||}Symbiotica, School of Anatomy, Physiology and Human Biology, University of Western Australia, Perth, WA 6009, Australia

Supporting Information

ABSTRACT: Plant-derived cellulose scaffolds constitute a highly viable and interesting biomaterial. They retain a high flexibility in shape and structure, present the ability to tune surface biochemistry, display a high degree of biocompatibility, exhibit vascularization, and are widely available and easily produced. What is also immediately clear is that pre-existing cellulose structures in plants can also provide candidates for specific tissue engineering applications. Here, we report a new preparation and fabrication approach for producing large scale scaffolds with customizable macroscopic structures that support cell attachment and invasion both in vitro and in vivo. This new fabrication method significantly improves cell attachment compared to that in our previous work. Moreover, the materials remain highly biocompatible and retain vascularization properties in vivo. We present proof-of-concept studies that demonstrate how hydrogels can be temporarily or permanently cast onto the macroscopic scaffolds to create composite plant-derived cellulose biomaterials. This inverse molding approach allows us to provide temporary or permanent biochemical cues to invading cells in vitro. The development of a new-generation of rapidly and efficiently produced composite plant-derived biomaterials provides an important proof that such biomaterials have the potential for numerous applications in tissue engineering.

KEYWORDS: biomaterials, cellulose, plants, scaffolds, biocompatibility, angiogenesis



INTRODUCTION

Designing biomaterials that support cell growth and function is essential for tissue engineering and regenerative medicine. As such, biomaterials are often designed to be intricate constructs with tunable structural, chemical, and mechanical properties.¹ Moreover, substantial research has focused on developing 3D biomaterials that resemble the complex in vivo cellular microenvironment.²

Biomaterials typically consist of two main classes: synthetic and naturally derived scaffolds.^{3,4} The synthetic biomaterials are often constructed with the use of synthetic polymers that mimic structural characteristics of the extracellular matrix (ECM), sometimes even functionalized with ECM proteins.⁵ On the other hand, naturally derived scaffolds involve repurposing existing biological materials and structures.⁶ Natural biomaterials can often be acquired using decellularization techniques.⁷ Decellularization refers to the process of removing the existing cellular structures while leaving behind an intact ECM.⁸ The remaining ECM is then used as a 3D biocompatible scaffold.⁹

For many years there has been a significant interest in synthetic, bacterial, and plant-derived cellulose as a potential biomaterial for tissue engineering applications.^{10–27} Cellulose is widely available in many forms and easily incorporated into

composite materials. It is now well established that bacterial and synthetic cellulose can act as scaffolds in a variety of tissue engineering applications, both in vitro and in vivo.^{28–30} Importantly, synthetic/bacterial cellulose is often molded or cast into a desired shape, and requires synthesis or cell culture protocols to produce scaffolds.³¹ On the other hand, the pre-existing structures of plant-derived cellulose scaffolds can be exploited directly with minimal processing and expense.^{32,33}

Several years ago, we demonstrated that native plant tissue can be decellularized, and the remaining cellulose scaffold can be used as a suitable platform for in vitro mammalian cell culture and also as an implantable in vivo biomaterial.^{32,33} Our work^{32,33} and recent studies^{34,35} have shown that a multitude of plant-derived cellulose scaffolds are suitable in vitro. The choice of the specific plant depends on the chemical, physical, and mechanical properties of the plant and the intended application.^{32–35} Although not necessary for in vitro cell growth, biofunctionalizations of the plant-derived cellulose

Special Issue: Biomaterials in Canada

Received: February 13, 2018

Accepted: March 2, 2018

Published: March 2, 2018

scaffolds have also been employed as steps in preparing cellulose scaffolds as we and others have shown.^{32,34,35} In addition, the similarities between the vascular structures of plants and animal tissues have been exploited via perfusion-based decellularization.³⁵ However, as shown previously, the need for a pre-existing vascular template is not a requirement for the vascularization of plant-derived cellulose biomaterials *in vivo*. In fact, we showed that decellularized, yet otherwise unmodified, plant cellulose is biocompatible and pro-angiogenic *in vivo*.³³ In this case,³³ vascularization occurs in the highly amorphous and porous plant-derived cellulose scaffolds without any necessary functionalization or dependence on pre-existing vascular structures.

Extending our previous work, we report here a new preparation and fabrication approach for producing large scale scaffolds with predefined structures and improved cell attachment and invasion, both *in vitro* and *in vivo*. Specifically, we demonstrate that apple-derived scaffold biomaterials can be hand- or machine-cut into desired shapes as opposed to approaches that might rely on the use of 3D printing, molding, or casting.^{7,8} We also present proof-of-principle studies that demonstrate how hydrogels can be temporarily or permanently cast onto the macroscopic scaffolds. Similar approaches have been employed in tissue engineering;^{36,37} however, to our knowledge, this is first time they have been used in combination with decellularized plant scaffolds. These “inverse molding” approaches allowed us to provide temporary or permanent biochemical cues to invading cells *in vitro*.

Moving beyond simple *in vitro* studies of plant-derived cellulose scaffolds, we also demonstrate that these biomaterials maintain their ability to become vascularized *in vivo* while improving cell invasion as compared to our previous *in vivo* study.³³ We show that these plant-derived cellulose scaffolds continue to display high biocompatibility *in vitro* and *in vivo*, with cell invasion occurring much more rapidly and completely.³³ Using decellularized cellulose scaffolds as biomaterials is a promising approach because of their availability, versatility, and ease of use.^{32–35} What is also immediately clear is that pre-existing cellulose structures in plants can also provide candidates for specific tissue engineering applications.

The results of this study and our previous work^{32,33} suggest cellulose scaffolds constitute a highly viable and interesting biomaterial. Specifically, they tend to overcome many of the complications that often arise with other traditional biomaterials while also retaining a high flexibility in shape and structure, presenting the ability to tune surface biochemistry, displaying a high degree of biocompatibility, exhibiting vascularization, and being widely available and easily produced. This is the first time that this new-generation of plant-derived biomaterial has been combined with hydrogels. These composite cellulose-based biomaterials provide a very important proof that such a platform can potentially be applied to many tissue engineering applications. The new fabrication process reported here is simple and supports high cell growth. Moreover, the processes and protocols described in our study, really open up dramatic new possibilities for biomaterial engineering with respect to the large size and geometric complexity that are now attainable. The biomaterials we describe are simply produced by hand or even on a computerized numerical control (CNC) machine within minutes without molding, complex chemistry, or restrictions to small sizes. The materials for these composites are easily and

cheaply sourced, biocompatible *in vitro*, and once implanted, are biocompatible and display clear vascularization. No special coatings or functionalization is required, and all studies were conducted in immune-competent animals. This study contributes many significant advantages to the field and opens up new possibilities for existing hydrogels and biopolymers to be used in combination with plant-derived cellulose biomaterials.

RESULTS

Improving Cell Attachment on Minimally Processed Plant-Derived Cellulose Scaffolds. Decellularization with the surfactant sodium dodecyl sulfate (SDS) was used to obtain 3D cellulose scaffolds void of any native apple cells or nucleic acids.^{32,33} With smaller scaffolds (as used previously^{32,33}), the concentration of SDS required was low; however, larger objects require higher concentrations of SDS to undergo complete decellularization.^{2,6,7,34,35} We found that the removal of all remaining SDS at higher concentration very time-consuming through washing alone. Here, a Ca²⁺ salt buffer was added to induce phase separation of the detergent due to a change in cloud point. This was carried out after washing steps to further remove any residual SDS.³⁸ However, due to the need of a sufficiently high salt concentration to stimulate micelle formation,³⁹ a salt residue does form on the cellulose surfaces (Figure 1A). The resulting salt residue was then removed by incubating the scaffold in dH₂O (Figure 1B), though several other techniques were found to be effective, such as incubation with acetic acid or DMSO or through sonication (data not shown). A significantly increased number of cells was found to attach to the scaffolds after treatment as compared to the control (Figures 1C and D). Two days after the cells were seeded onto the biomaterial, cell density was quantified with the use of the CCK-8 cell counting kit (Figure 1E). A significantly greater number of cells were found attached to the treated scaffolds ($3.7 \times 10^1 \pm 2.9$ cells/mm³) compared to that found on the controls ($2.6 \times 10^1 \pm 2.5$ cells/mm³) ($P = 1.8 \times 10^{-2}$, $N = 5$). We also showed that when preparing small biomaterial constructs, the remnant SDS can alternatively be removed with extensive washing without using the salt pretreatment, and a comparable viable cell attachment can be achieved; this method is time-consuming and ineffective with larger samples (Supporting Information Figure S1) ($P = 9.2 \times 10^{-1}$, $N = 4$).

Construction of Macroscopic Cellulose Scaffolds and Surface Modification. Here, we show how decellularized cellulose can be further processed by cutting them into macroscopic ring shapes from bulk hypanthium tissue (Figure 2). Many studies produce large scaffolds utilizing gel casting or 3D printing techniques.³⁶ Here, as a proof-of-concept, we created ring shaped scaffolds (Figure 2). A ring was chosen simply as a model of a complex feature that would typically be created through other techniques. Of course, a broad array of desired shapes can conceivably be created (Supporting Information Figure S2). Although the ring was chosen only as a proof-of-concept structure, this shape has complex properties that are of significant biological relevance. The ring contains two flat faces, two curved surfaces, two radii of curvature, four sharp edges connecting each face to the curved surfaces, and a porous 3D interior (Figure 2).

First an apple was sliced into thin (1.2 mm sections) using a mandolin slicer (Figure 2A). A 5 mm diameter disk with a 1.2 mm thickness was then carved out of the slice using a 5 mm biopsy punch. To complete the ring, a 2 mm biopsy punch was

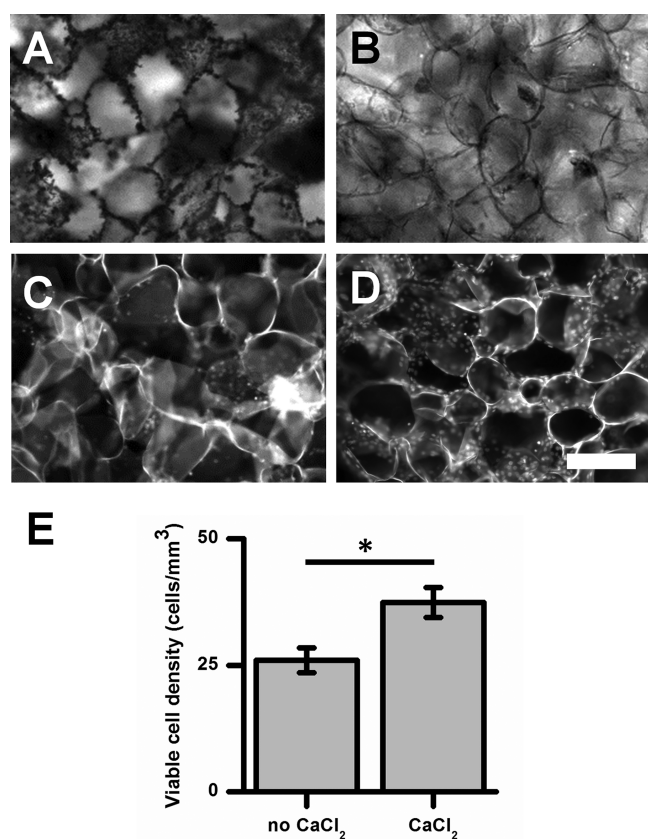


Figure 1. CaCl₂ pretreatment. (A) CaCl₂ pretreatment was used to remove remnant surfactant from the scaffold. (A) The salt/micelles crash out of solution onto the scaffold. (B) Removal of the salt residue. (C) C2C12 myoblasts cultured on the scaffold without the CaCl₂ pretreatment. (D) C2C12 myoblasts cultured on the scaffold with the CaCl₂ pretreatment. (E) CCK-8 quantification of cell density shows an increased number of viable cells attached to the SDS + salt treated scaffolds ($3.7 \times 10^1 \pm 2.9$ cells/mm³) compared to SDS alone ($2.6 \times 10^1 \pm 2.5$ cells/mm³) ($P = 1.8 \times 10^{-2}$, $N = 5$) after 2 days of culture. All values are mean \pm SEM. Scale = 200 μ m.

used to remove a 2 mm disk from the center of the 5 mm disk (Figure 2B). After fabrication, the samples were transferred to a 0.1% SDS solution and decellularized as described above for 48 h while being shaken at 180 rpm (Figure 2C). A distinct change in transparency was observed during decellularization.

C2C12 mouse myoblast cells were seeded onto the scaffolds, and the cells were allowed to proliferate and invade the structure for 2 weeks (Figure 2D and Figure 3). After 2 weeks, the rings were found to be completely invaded by cells (Figure 3). We note that at this stage, no deliberate surface functionalization has been required to achieve these results as opposed to other studies.^{34,35} These results demonstrate that complex 3D cellular constructs can be simply produced in plant-derived cellulose scaffolds.

The ring scaffolds also present another potential use in tissue engineering applications. We now show that hydrogels can be cast onto the macroscopic structure, after which the gel assumes the shape of the scaffold itself as opposed to the traditional approach of casting hydrogels into molds.^{29,40,41} In this inverse molding scenario, we chose to cast a gelatin or collagen hydrogel onto the scaffolds simply to demonstrate feasibility (Figure 3). In the case of gelatin hydrogels, a 10% (m/v) gelatin solution in Dulbecco's modified Eagle's medium

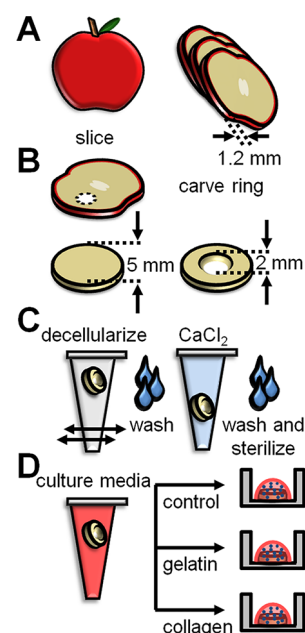


Figure 2. Schematic of biomaterial preparation. (A) The apple was cut and sliced on a Mandolin slicer. (B) A 5 mm biopsy punch was used to cut out a disk from the apple slice; a 2 mm biopsy punch was used to cut out a disk from the 5 mm disk to make the ring. (C) The ring was decellularized in 0.1% SDS for 48 h, washed, incubated with salt buffer for 24 h, and washed and sterilized. (D) Seeding the scaffold with cells in media, gelatin, and collagen.

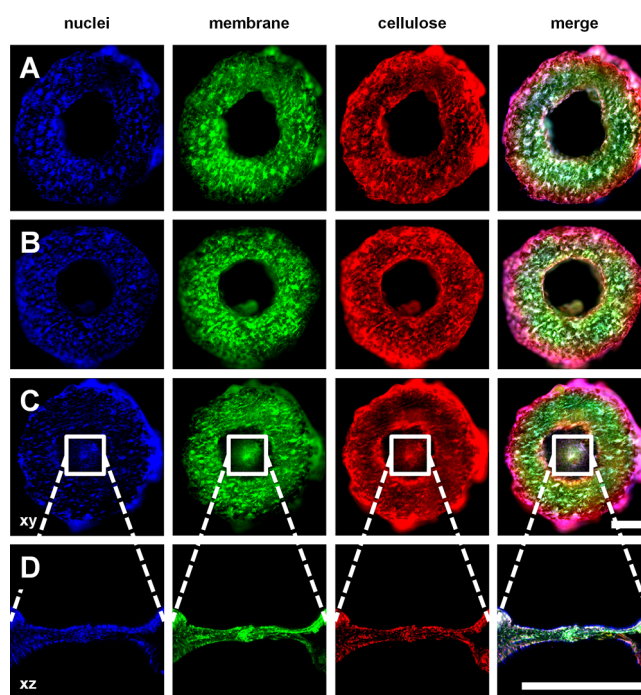


Figure 3. Ring structures with temporary and permanent hydrogels. C2C12 myoblasts were grown on the ring scaffolds for 2 weeks after being seeded with culture media (A), gelatin (B), and collagen (C and D). The scaffolds were stained for the nuclei (blue), cell membrane (green), and cellulose (red), and imaged using confocal microscopy. The permanent collagen hydrogel created a compacted collagen suspension over the ring-hole (C and D). It should be noted that the collagen gel suspended over the ring-hole contained cells as well. Scale = 1000 μ m.

(DMEM) was first prepared. Gelatin has a melting temperature of 32 °C;⁴² therefore, the gelatin solution was kept at 37 °C to remain in its liquid state until the cells were introduced into the solution and the gelatin-cell suspension was cast around the cellulose ring (Figure 2D). The gelatin solution then cooled below its melting temperature and was left to gel for 15 min at room temperature. Here, the hydrogel containing the cells was left on the scaffold in its gelled state for a further 45 min. Following this period, the sample was immersed in culture media and placed in the incubator at 37 °C and 5% CO₂. Once above the melting temperature, the gelatin gel slowly diffuses out of the scaffold while the cells remain on the biomaterial (Figure 3B). In this temporary inverse molding scenario, the cells are temporarily exposed to a distinct biochemical cue during the attachment process.

Conversely, the cellulose scaffold can also act as an inverse mold for permanent gels. Cellulose rings were covered in a 1.5 mg/mL collagen solution containing cells in a method very similar to the gelatin scenario (Figure 2D). The collagen solution rapidly polymerizes and forms a permanent gel containing the biomaterial and the cells. After 15 min of incubation at room temperature, culture media was added to the collagen coated cellulose ring. The sample was then placed in the incubator at 37 °C and 5% CO₂. After incubation, the collagen gel was not observed to melt (as expected) and was also found to fill the hole in the ring as a compacted structure (Figures 3C and D). This creates a composite biomaterial in which cells are found in two distinct regions: in the cellulose and collagen ring or in the collagen gel suspended in the ring-hole.

Cell Invasion and Proliferation. The CCK-8 assay was used to quantify and compare the initial attachment of the cells (one day postseeding) on the scaffolds with the temporary and permanent hydrogels. It was found that a significantly greater population of viable cells remained in the biomaterial used in combination with the permanent hydrogel (Figure 4) ($P = 1.2 \times 10^{-3}$ and $P = 1.1 \times 10^{-2}$ for the collagen compared to the control and gelatin samples respectively, $N = 4$). The CCK-8 cell counting kit is a powerful assay used to measure cell proliferation and viability; however, there is a maximum number of cells that can be detected. After two weeks of cell growth, the number of cells on the biomaterial exceeded the detection limit of the CCK-8 assay. As a result, the live:dead cell ratio was calculated to further assess the biocompatibility of the cellulose-based biomaterials ($N = 3$ scaffolds for each condition). After 2 weeks, no statistically significant difference in the ratio of live:dead cells was observed (Figure 4) ($P > 0.05$, $N = 6$ images for each condition), and the spatial distribution of the live and dead cells were uniform for the limit of detection.

In addition to assessing the in vitro biocompatibility, the mechanical properties of the biomaterial were also investigated (Supporting Information Figure S3). Employing bulk compression testing, the Young's moduli of the scaffolds were measured after two weeks of culture using a custom-built device. The Young's modulus of the scaffolds without the CaCl₂ treatment (8.0 ± 1.7 kPa) was significantly lower than that of the treated samples ($1.7 \times 10^1 \pm 1.1$ kPa) ($P = 4.9 \times 10^{-2}$, no CaCl₂: $N = 5$, CaCl₂: $N = 6$). Moreover, although the addition of the hydrogels did increase the moduli, they were not significantly different from the CaCl₂-treated scaffolds ($1.5 \times 10^1 \pm 3.6$ kPa, $2.3 \times 10^1 \pm 1.7$ kPa, gelatin and collagen respectively, $P > 0.05$, $N = 6$). Importantly, the mechanical

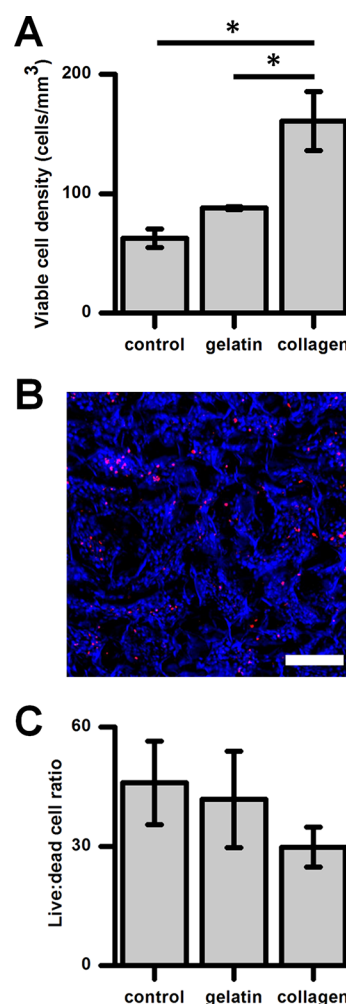


Figure 4. Initial cell attachment and viability. (A) The initial attachment of the cells one day postseeding was quantified using CCK-8. A significantly greater initial cell density was obtained with the permanent collagen hydrogel ($P = 1.2 \times 10^{-3}$ and $P = 1.1 \times 10^{-2}$ for the collagen compared to that obtained with the control and gelatin samples, respectively, $N = 4$). (B) The cells on the biomaterials were stained after 2 weeks of culture with Hoechst 33342 (stains all cell nuclei) and propidium iodide (stains only dead cell nuclei) and were imaged with confocal microscopy to assess cell viability ($N = 3$ scaffolds for each condition). Scale = 200 μ m. (C) No statistically significant difference in the ratio of live:dead cells was observed ($P > 0.05$, $N = 6$ images for each condition).

properties of all the scaffolds fall well within the range of native animal tissues such as muscle.^{44,45}

Confocal laser scanning microscopy was used to image the top and bottom of the scaffolds after cells were allowed to proliferate for 2 weeks ($N = 6$ scaffolds for each condition). Both sides of the ring were imaged to confirm that cell invasion was similar on both faces, revealing complete penetration. Figures 5A–C shows the XY and ZY projections of the cells on the cellulose biomaterial. The nuclei of the cells were found along the cellulose cell walls. Orthogonal views of confocal scans reveal that the cells invaded the scaffold to the limit of detection (~ 300 μ m imaging depth). To assess how well cells penetrated the entire 1.2 mm thickness of the biomaterial, the scaffolds were also cut perpendicular to the ring diameter (Figure 5D), and the cross-sectional areas of the rings were imaged ($N = 3$) (Figures 5E–G). Confocal imaging for cell

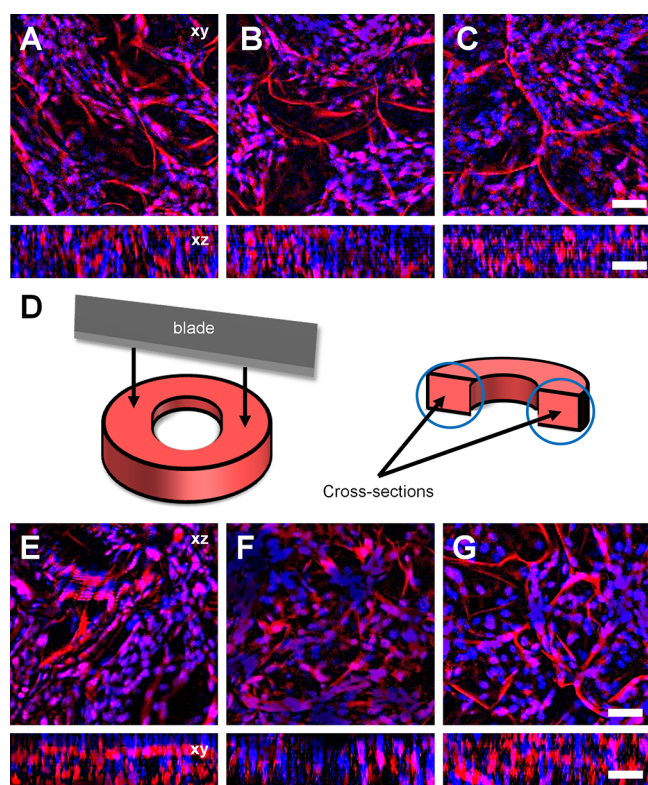


Figure 5. Cell invasion and proliferation. (A–C) XY and XZ maximum projection confocal images of C2C12 myoblasts on the ring scaffolds. C2C12 myoblasts were grown on the ring scaffolds for two weeks after being seeded with culture media (A), gelatin (B), and collagen (C). (D) The rings were cut with a razor blade to expose the cross-sectional areas. (E–G) Cross-sectional areas XZ and XY maximum projections of confocal images of the control (E), gelatin (F), and collagen (G) biomaterials. Blue = nuclei, red = cellulose. Scale = 50 μm .

invasion and proliferation revealed similar cell density under all conditions reported above. Quantification of confocal data allowed the number of cells in randomly selected $2.7 \times 10^7 \mu\text{m}^3$ volumes to be calculated. We observed no statistical differences in cell numbers under any of the three ring fabrication conditions ($P > 0.05$, $N = 12$ images for each condition) (Supporting Information Figure S4). Importantly, temporary and permanent inverse molding does not appear to impair cell proliferation after two weeks of culture when compared to bare scaffolds. However, it should also be noted that C2C12 myoblasts deposit their own ECM when cultured on 3D scaffolds.⁴³ Consequently, the three different techniques (bare scaffold, temporary gelatin functionalization, and permanent collagen functionalization) can be used interchangeably without affecting cell invasion and proliferation in the scaffolds with the particular size and geometry used in this study, all while exposing cells to three distinct biochemical cues. The result of this proof-of-concept study is that the decellularized cellulose biomaterials can be used in combination with temporary and permanent inverse molding hydrogel techniques. Naturally, this concept is not restricted to gelatin and collagen: a wide variety of temporary and permanent biochemical cues can be supplied through the use of other polymers, proteins, and biomolecules. The use of specific proteins will of course depend on the goals and interests of individual investigators who might employ this approach.

Total cell growth after two weeks was not statistically different under the three conditions described here. As a result, the two week time period was sufficient for full invasion of the biomaterials used in this study. However, when compared to our original protocol,³² a drastic improvement in the cell invasion and proliferation is apparent. After 2 weeks, the samples with the calcium chloride incubation purification process ($1.5 \times 10^2 \pm 8.2$ cells) showed comparable cell invasion ($P = 3.4 \times 10^{-1}$, $N = 3$) to that of our previous study after 12 weeks ($1.8 \times 10^2 \pm 2.3 \times 10^1$ cells) despite the greater cell density seeding used in our previous study.

In Vivo Biocompatibility of Subcutaneously Implanted Scaffolds. We next sought to confirm that the addition of the salt treatment to our protocol did not create any negative impact in vivo, however unlikely.³³ Although we have shown that the scaffolds support cell growth in vitro, a true test of biocompatibility requires an in vivo study. Here, we subcutaneously implanted salt treated plant-derived cellulose scaffolds under the skin of wild-type mice ($N = 8$ mice with two $5 \times 5 \times 1.2$ mm scaffolds implanted per mouse). As with our original subcutaneous study which employed a different decellularization protocol,³³ here there were no cases of mice exhibiting behavior indicative of pain induced by the cellulose scaffold throughout the study. The cellulose constructs were then resected after four weeks. Histological analysis was used to investigate the cell infiltration, proliferation, collagen deposition, and angiogenesis. Importantly, four weeks postimplantation, healthy tissue can be observed surrounding the cellulose scaffold. Moreover, significant cell infiltration into the scaffold is readily apparent (Figure 6). In fact, the inclusion of a CaCl_2 buffer in our preparation promoted greater cell proliferation and invasion compared to our previous report.³³ The scaffolds also displayed vascularization, which is reflected in a number of clearly visible blood vessels (with blood cells) in the Masson's Trichrome images (Figures 6A–C). We further confirmed vascularization with CD-31 staining for endothelial cells

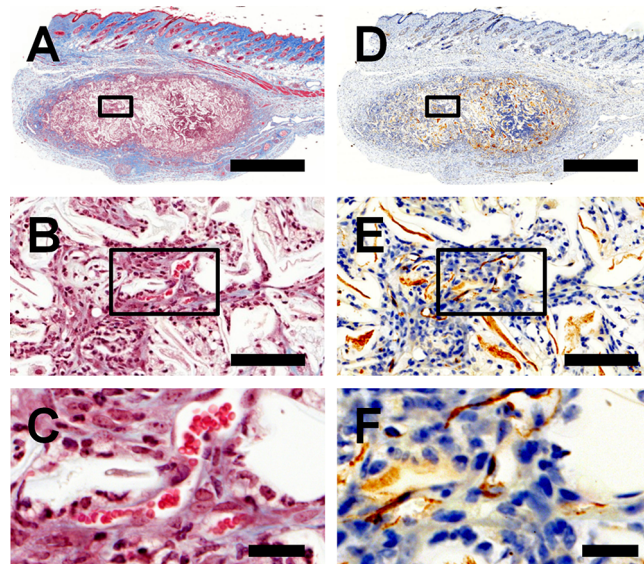


Figure 6. In vivo biocompatibility of CaCl_2 treated samples. Cross-sectional images of decellularized apples treated with CaCl_2 subcutaneously implanted into mice for four weeks. Samples were stained with Masson's Trichrome (A–C) and CD 31 (D–F). Scale for A and D = 1000 μm . Scale for B and E = 100 μm . Scale for C and F = 25 μm .

(Figures 6D–F). It is important to recognize that vascularization was able to occur even in the absence of any templating physical structures or need for biochemical functionalization of the cellulose scaffolds with pro-angiogenic factors. These results confirm the biocompatibility of salt treated plant-derived cellulose scaffolds and indicate their applicability as a possible platform for tissue-engineering applications. While we explored the use of inverse molding techniques for hydrogels, gelatin and collagen functionalization were only employed as a proof-of-concept rather than an end-product or application of these materials. Ultimately, investigators will have to assess the *in vitro* and *in vivo* biocompatibility of any cellulose scaffold functionalized with their target biomolecules in a manner as described above.

DISCUSSION

The use of cellulose scaffolds as biomaterials has many advantages such as low cost, ease of production, biocompatibility, functionalization, tunable mechanical properties, and successful subdermal implantation within relatively static tissues. In recent years, there have been major advances in 3D cell culture and scaffolding techniques that aim to capture the complexity of the *in vivo* microenvironment.^{46,47} Numerous methods have now been developed for the production of biomaterial scaffolds for tissue engineering and regenerative medicine applications, each with their own benefits and drawbacks.^{46,47} In general, biomaterial scaffolds should provide structural support, promote cell invasion and proliferation, prevent or minimize severe immune responses, and be pro-angiogenic and induce vascularization of the scaffold to support cellular function.

Several years ago, we pioneered the production of biomaterials derived directly from plants and proved the efficacy both *in vitro* and *in vivo*.^{32,33} This early work has now inspired other recent studies.^{34,35} Biomaterials derived directly from plants carry several interesting advantages, including straightforward production methods, widespread availability of material, and the potential for utilizing pre-existing microstructures within plant tissues.^{32,33} Moreover, we showed that the cellulose-based biomaterials remain stable *in vivo*.³³ Taken together, it is now clear that many cell types will attach and proliferate on plant-derived cellulose scaffolds. In recent work, the contraction of a small group of cardiac cells was examined on leaf cellulose scaffolds.³⁵ However, it was clear from the study that the scaffolds appeared unable to support complete invasion and proliferation. As revealed in the same study, the contractile dynamics of cardiac cells were impaired on cellulose scaffolds as compared to those on traditional substrates and biomaterials.^{35,48,49} These results point to the need for robust strategies for the preparation of plant-derived cellulose scaffolds that are optimized for a high degree of cellular invasion and proliferation both *in vitro* and *in vivo*.

Here, we present a preparation and fabrication approach for producing highly novel macroscopic plant-derived cellulose scaffolds with predefined structures. For the first time, we demonstrate that this new-generation of plant-derived biomaterials can be combined with hydrogels. Consequently, this study establishes a platform that can potentially be applied to many tissue engineering applications. This new platform for composite cellulose biomaterials combines the advantages of hydrogel-based biomaterials with the ease of production and efficiency of the cellulose-based scaffolds. In this proof-of-concept study, we show how plant-based scaffolds with

complex features can be hand- or machine-crafted and then repurposed for new biological characteristics.

The anionic detergent SDS was used to decellularize the apple hypanthium tissue to obtain the cellulose scaffold.^{7,32} Hence, an effective way to remove SDS prior to cell seeding was required. In this study, we added a salt treatment to our previous protocol to promote any residual SDS molecules to form micelles.³⁸ Several salt buffers can accomplish this task, but divalent cations form tighter micelles than their monovalent counterparts.³⁸ The addition of the salt alters the critical micelle concentration of the surfactant;³⁹ at a certain concentration known as the cloud point, a phase transition occurs, and the micelles become insoluble and can be easily washed away.⁵⁰ The salt treatment can be useful in cases where simple washing is not practical. For instance, large 3D constructs (several centimeters in size) can require high concentrations of SDS (~5%) for complete decellularization (Supporting Information Figure S2). This high concentration of SDS makes removing remnant surfactant difficult. Recently, two other studies have taken advantage of the structures of decellularized plant tissues for 3D mammalian cell culture.^{34,35} In these studies, harsh decellularization conditions were used to render the scaffold free of the native plant cells and nuclear content.^{34,35} Moreover, both studies show incomplete cell proliferation and invasion of the plant-derived constructs. It is possible that remnant detergents and chemicals are responsible for the incomplete invasion of the scaffolds; however, experimental validation is required to confirm this speculation. Importantly, it also remains unclear if the production methods described in these previous studies result in biocompatible and pro-angiogenic scaffolds *in vivo* as animal studies were not carried out by the authors.^{34,35} The new fabrication process reported here is simple and supports high cell growth. Moreover, the processes and protocols described in our study, really open up dramatic new possibilities for biomaterial engineering with respect to the large size and geometric complexity that are now attainable. The biomaterials we describe are simply produced by hand or even on a CNC machine within minutes, without molding, complex chemistry, or restrictions to small sizes.

Many synthetic 3D biomaterials rely on molding techniques to achieve their intended shape.⁵¹ An advantage of using decellularized plant cellulose as a 3D biomaterial is that it can simply be cut into the desired shape. Here, we demonstrated the production of cellulose rings as scaffolds for tissue engineering *in vivo*. Of course, the maximum size of the construct (without any further processing) will be limited by the plant being employed as a starting material. We presented proof-of-concept studies to show how the versatility of the biomaterial can be further increased by casting temporary or permanent hydrogels onto the macroscopic scaffolds with inverse molding techniques.⁵¹ While this technique has been previously applied to synthetic tissue engineering,^{36,37} this appears to be the first time this has been used to exploit the pre-existing structures of plants. This approach allowed us to provide temporary or permanent biochemical cues to the invading cells. The molding techniques can be particularly useful if intricate features of the biomaterial need to be populated with cells. Conventionally, cells are suspended in culture media and are seeded onto the substrate.⁵² The cell culture media is of low viscosity; therefore, the media can easily pass through the porous scaffold without allowing enough time for cell attachment. This problem can be overcome by using temporary or permanent inverse molding techniques. Tempo-

rary molding is advantageous when a standalone cellulose biomaterial with complex features is desired. As evidenced by our gelatin experiments, the temporary mold can extend the time the cells are in contact with the biomaterial and then melt away after its function is complete. Moreover, the temporary mold can supply biochemical cues to the cells that are desirable for only a short period of time. On the other hand, in other scenarios it is desirable to create a permanent gel encompassing the biomaterial. Unlike gelatin, collagen remains in its gel state at 37 °C, which is particularly useful for cell culture applications that require a permanent gel or persistent biochemical cues.

Importantly, cell invasion was comparable for the three different conditions: bare cellulose, gelatin temporary mold, and collagen permanent mold. The significance of these findings is that the same result can be obtained regardless of the molding technique that is used. As this work and our previous studies^{32,33} demonstrate, plant-derived cellulose scaffolds are inert and simply provide a stable 3D structure on which cells can proliferate and function. Therefore, the choice of biofunctionalization seeding technique depends on the intended application of the material. It should be noted that different cells deposit and require varying extracellular matrixes.⁴³ Therefore, the outcome of using the plant-based decellularized biomaterial in conjunction with hydrogels containing cells that produce an insufficient ECM may increase cell invasion and proliferation in comparison to culturing the cells on bare scaffolds. Our *in vitro* results reveal that the scaffolds are highly biocompatible. The live:dead cell ratios confirm the presence of mostly viable cells. However, we urge researchers to employ caution when interpreting the results of the live and dead cell experiments. The scaffold size and geometry used here certainly affect the results. Although not found in this study, we do expect a necrotic core to be present in larger biomaterials with insufficient porosity or without supplemented perfusion as a result of hypoxia and inadequate diffusion of metabolites.⁵³ When compared to the physiological condition at approximately 1×10^8 cells/mL,⁵⁴ our *in vitro* experiments have a lower cell density. Nevertheless, our *in vivo* results show a relatively high cell density, similar to that of the surrounding native tissue. Many factors influence cell density such as cell type, mechanical properties, structural characteristics, and biochemical features. It should be noted that our motivation for presenting these proof-of-principle experiments was to establish a potential tissue engineering platform with plant-derived cellulose scaffolds. Increasing the cell seeding density to approach the physiological limit or determining the maximum limit was unnecessary; the *in vivo* results address this issue. It is important to note that matching cell density *in vitro* is not our end goal. Rather, we are developing implantable biomaterials; therefore, *in vivo* biocompatibility, vascularization, and cell invasion are of primary concern. In future work, specific tissue engineering goals will be examined, as opposed to fully exploring the landscape of possibilities of employing gelatin/collagen in the present study. To that end, the composite material can be selected to match the mechanical and physical properties of the local microenvironment. In our case, the gelatin and collagen hydrogels did not appear to alter the pore size or pore size distribution of the cellulose pores, consistent with our previous studies.^{32,33} Obviously, the physical properties such as porosity depend on the choice of the material. Here the choice of composite material was arbitrary; extensive characterization of the physical properties was unnecessary. Nevertheless, the mechanical properties are of

significant interest; thus, the Young's modulus was quantified. Interestingly, the treatment with the CaCl₂ increased the Young's modulus, while the addition of the hydrogels did not have a significant effect. The increase in the Young's modulus after the salt treatment was likely the result of remnant salt adsorbed on the surface. We note, however, the mechanical properties of the scaffolds which vary between ~5–20 kPa fall well within the range of native animal tissues such as muscle.^{44,45}

Our *in vivo* results also show that the scaffolds never become calcified or fibrotic. Rather, collagen matrix deposition is observed concomitantly with extensive cell invasion.³³ Crucially, the plant-derived cellulose biomaterial exhibited vascularization, which results in the formation of blood vessels that supply the invading cells with nutrients. Apple hypanthium tissue is highly porous and sponge-like in structure and lacks the presence of pre-existing vascular structures which might act as a template for blood vessel formation. Despite this, and existing hypotheses that such templating structures are important,^{29,35,41} we show that such pre-existing structures are not a requirement for vascularization. In fact, it is likely that the highly porous nature of plant-derived cellulose biomaterials is the critical element which promotes vascularization.⁵⁵ Although plant-derived cellulose scaffolds are stable and robust as subdermal implants and in tissues/structures that are relatively stable,³³ it is unclear how applicable they will be in applications that involve the repair of cardiac and/or muscle tissues. Such tissues are mechanically dynamic, which leads to the application of large stresses to any implanted biomaterial. Plant-derived cellulose scaffolds, without any further processing, are highly brittle and likely inappropriate for such applications, especially when other more effective biomaterials have already been developed.^{56,57} It is also unclear at this point if such plant-derived cellulose scaffolds will be effective for *de novo* organ engineering. At present, these materials do appear to be highly effective in tissue engineering/repair strategies within certain criteria as discussed here. Future studies will continue to elucidate the full potential of these plant-derived cellulose biomaterials in regenerative medicine.

Combining the scaffold with hydrogels expands the potential applications of these materials, and we anticipate this work will have significant impacts in the field. We stress that this study is a proof-of-concept study that will provide the foundation for more sophisticated investigations in the near future. Improved cell adhesion, both *in vitro* and *in vivo*, combined with inverse molding provides an important platform for future tissue engineering applications. The materials for these composites are easily and cheaply sourced, biocompatible *in vitro* and *in vivo*, and display clear vascularization. This study opens up new possibilities for existing hydrogels and biopolymers to be used in combinations with plant-derived cellulose biomaterials. The choice of gelatin and collagen as the comparison materials was quite arbitrary as there are many biomaterials available. The combination of scaffolds with temporary or permanent hydrogels will be useful in delivering biochemical cues (matrix proteins, growth factors, small molecules, etc.) to attract or promote the growth of specific cell types. Control over the organization and invasion of specific cell types remains an important challenge in 3D tissue engineering. Future work will focus on combining the inverse molding techniques with *in vivo* experiments to direct and template specific cells in 3D space. Nevertheless, emerging plant-derived cellulose scaffolds present an affordable, accessible, easy to use, and versatile 3D

biomaterial that holds important promise for future applications. The simplistic approach to biomaterial fabrication is a very attractive feature of this novel biomaterial, and we anticipate that it will benefit the continued development of novel biomaterials by many different research groups.

MATERIALS AND METHODS

Scaffold Production. A mandolin slicer was used to slice McIntosh Red apples (Canada Fancy) into thin 1.2 mm sections, measured with a Vernier caliper. A 5 mm diameter disk with a 1.2 mm thickness was then carved out of the hypanthium tissue of the slice using a 5 mm biopsy punch. A 2 mm biopsy punch was used to remove a 2 mm disk from the center of the 5 mm disk. Thus, a macroscopic ring was obtained with an inner diameter of 2 mm, an outer diameter of 5 mm, and a thickness of 1.2 mm. The samples were transferred to a 0.1% SDS solution and decellularized for 48 h while being shaken at 180 rpm. After decellularization, the samples were washed three times with dH₂O. Next, the rings were incubated in 100 mM CaCl₂ for 24 h at room temperature to remove any surfactant residue. The samples were washed three times with dH₂O to remove the salt residue and then were incubated with 70% ethanol for sterilization. After the removal of the ethanol, three washes with dH₂O were performed to yield a sterile ring free of contaminants. Alternatively, the samples can be autoclaved to be sterilized.

Cell Culture. C2C12 mouse myoblast cells were maintained at 37 °C and 5% CO₂. The cells were cultured in high glucose DMEM, supplemented with 10% fetal bovine serum and 1% penicillin/streptomycin (100 U/mL and 100 µg/mL respectively) (Hyclone Laboratories Inc.). The C2C12 myoblast cells cultured on cell culture plates were trypsinized and resuspended in DMEM. The cells were counted and centrifuged to separate the cells from the trypsin and the media. The supernatant was aspirated, and the pellet containing 5 × 10⁴ cells was resuspended in either fresh culture medium, a 10% (m/v) Porcine Type-A Gelatin (GE) (Sigma-Aldrich) solution in culture medium, or a 1.5 mg/mL collagen solution. The collagen gel was made by mixing 50% (v/v) of 3 mg/mL type I collagen (Gibco) with 1.25% of 1 N NaOH, 10% of 150 mM D-ribose, 1% FBS, 10% of 10× DMEM, and 27.25% autoclaved dH₂O at 4 °C. In each condition, C2C12 mouse myoblast cells were seeded onto the biomaterial, and the cells were allowed to proliferate and invade the scaffold for two weeks. The culture medium was replaced every two days, and the samples were transferred to new culture plates after one week of growth.

The GE solution was used as a temporary inverse mold. The resuspension in the GE solution was performed at 37 °C. After the gelatin–cell solution was pipetted onto the scaffold, the gelatin solution cooled below its melting temperature and was left to gel for 15 min at room temperature. Here, the hydrogel containing the cells was left on the scaffold in its gelled state for a further 45 min. Following this period, 2 mL of room temperature cell culture medium was added to the Petri dish containing the gelatin coated ring. The sample was then placed in the incubator at 37 °C and 5% CO₂.

The collagen solution was used as a permanent inverse mold. Here, the inverse principle applied: the gel was in its liquid form at 4 °C and solidified at room temperature. A collagen gel–cell mixture was produced by resuspending the pellet of cells in a 4 °C collagen solution. The collagen solution rapidly polymerizes within 5 min and formed a permanent gel containing the biomaterial and the cells. After 15 min of incubation at room temperature, 2 mL of room temperature culture medium was added to the Petri dish containing the collagen coated ring. The sample was then placed in the incubator at 37 °C and 5% CO₂.

Staining. Prior to staining, the cells were washed 3 times with PBS and then fixed with 3.5% paraformaldehyde for 10 min. Staining of the decellularized apple scaffold was accomplished as described previously.^{32,58} Briefly, the samples were rinsed with water and incubated in 1% periodic acid (Sigma-Aldrich) at room temperature for 40 min. The tissue was rinsed again with water and incubated in Schiff reagent (100 mM sodium metabisulfite and 0.15 N HCl) with

100 µg/mL of propidium iodide (Invitrogen) for 2 h. The samples were then washed with PBS. The myoblast cell membranes and nuclei were stained with a solution of 5 µg/mL wheat germ agglutinin (WGA) 488 (Invitrogen) and 1 µg/mL Hoechst 33342 (Invitrogen) in PBS, respectively, for 30 min.

Microscopy. The cells and biomaterials were imaged with epi-fluorescence and laser scanning confocal microscopy. A Nikon Eclipse TiE epi-fluorescence and phase contrast microscope (Nikon, Canada) with a CCD camera (Photometric Cool Snap HQ²), and 4× and 10× objective lenses were used to image the biomaterials. In addition, the samples were imaged with a Nikon TiE A1-R high speed resonant scanner confocal microscope with a 10X objective. ImageJ (Fiji) was used to process the images. Confocal images presented here are maximum intensity projections of confocal volumes. Brightness/contrast settings were adjusted to maximize the fluorophore signal; otherwise, no other image manipulations were performed.

In Vitro Cell Invasion and Proliferation Quantification. Cell Counting Kit-8 (CCK-8) (Dojindo Molecular Technologies, Inc.) was used to measure the number of viable cells in the scaffold after the initial seeding. A standard curve ($R^2 = 0.998$) was produced by creating serial dilutions of 5 × 10⁴ cells with a dilution factor of 2 in a 96-well plate for a final volume of 100 µL of cells and media plus 10 µL of CCK-8 reagent after a preincubation of 12 h. The absorbance of the solution was measured at 450 nm after 3 h of incubation at 37 °C, 5% CO₂. For the experimental measurements, the rings were seeded with cells as described above, then transferred to a 96-well plate with 100 µL of media +10 µL of CCK-8 reagent after a preincubation period of 12 h. The absorbance of the solution was measured at 450 nm after 3 h of incubation at 37 °C, 5% CO₂. The values presented are mean values ± the standard error of the mean (SEM).

The confocal images of the cell nuclei were thresholded using the ImageJ (Fiji) adaptive threshold plug-in, and the analyze particles plug-in was used to measure the number cells in a 300 × 300 µm area (analysis after 2 days of culture) or a 300 × 300 × 300 µm volume (analysis after 2 weeks of culture). The values presented are mean values ± SEM.

Live:Dead Cell Analysis. After 2 weeks of culture, the scaffolds were incubated with 10 µg/mL of Hoechst 33342 (Invitrogen) and 1 µg/mL of propidium iodide (Invitrogen) for 20 min to stain the nuclei of the live and dead cells, respectively. The biomaterials were then imaged with confocal microscopy. The images of the cell nuclei were thresholded using the ImageJ (Fiji) adaptive threshold plug-in, and the analyze particles plug-in was used to measure the number cells. Here, the live:dead cell ratio expression is unitless. The values presented are mean values for multiple volumes ± SEM.

Young's Modulus. The Young's modulus was measured after 2 weeks of culture by compressing the material to a 10% strain, at a strain rate of 50 µm/s, using a custom-built compression device and LabVIEW software. The force–indentation curves were converted to stress–strain curves and fitted in Origin 8.5 to calculate the Young's modulus.

Animals. Wild-type immunocompetent C57BL/10ScSnJ mice (males and females; 6–9 weeks old; $N = 8$) were purchased from The Jackson Laboratory (Bar Harbor, Maine, United States) and bred in our facilities. The mice were housed at constant room temperature (22 °C) and humidity (52%), fed a normal chow diet, and kept under a controlled 12 h light/dark cycle. The subcutaneous implantation procedures and related protocols were approved by the Animal Care and Use Committee of the University of Ottawa.

Cellulose Implantation. The mice were anesthetized using 2% Isoflurane USP-PPC (Pharmaceutical partners of Canada, Richmond, ON, Canada). The eyes of the mice were kept from drying with the application of ophthalmic liquid gel (Alco Canada Inc., ON, Canada). The breathing of the mouse was constantly monitored to ensure that the animal was in the correct plane of anesthesia. The mouse dorsal ventral region was shaved with the underlying skin cleaned and sterilized using ENDURE 400 Scrub-Stat4 Surgical Scrub (chlorhexidine gluconate, 4% solution; Ecolab Inc., Minnesota, United States) and Soluprep (2% w/v chlorhexidine and 70% v/v isopropyl alcohol; 3 M Canada, London, ON, Canada). Animal hydration was maintained

via subcutaneous injection (s.c.) of 1 mL of 0.9% sodium chloride solution (Hospira, Montréal, QC, Canada) on the opposite side of the cellulose implantation site. Throughout the surgical procedures, the body temperature of the mouse was maintained at 37 °C to maximize recovery of the animal. All strict sterility measures were upheld for survival surgeries. To implant the scaffolds, two 8 mm incisions were cut on the dorsal section of each mouse (upper and lower). Two cellulose scaffold samples were separately and independently implanted into each mouse. The incisions were then sutured using Surgipro II monofilament polypropylene 6-0 (Covidien, Massachusetts, United States), and transdermal bupivacaine 2% (as monohydrate; Chiron Compounding Pharmacy Inc., Guelph, ON, Canada) was topically applied to the surgery sites to prevent infection. Additionally, buprenorphine (as HCL) (0.03 mg/mL; Chiron Compounding Pharmacy Inc. Guelph, ON, Canada) was administered s.c. as a pain reliever. All animals were then carefully monitored for the following three days by animal care services and received replicate pharmacological treatments.

Scaffold Resections. At four weeks postimplantation, the mice were euthanized using CO₂ inhalation and exsanguination via heart dissection. The dorsal skin was carefully resected and immediately immersed in sterile PBS solution. The underlying skin containing cellulose scaffolds was then photographed, cut, and fixed in 10% formalin for at least 48 h. The samples were then kept in 70% ethanol before being embedded in paraffin by the PALM Histology Core Facility of the University of Ottawa.

Histology. For histological analysis, serial 5 μm-thick sections starting 1 mm inside the cellulose scaffold were cut. The sections were stained with Masson's Trichrome. For immunocytochemistry, heat induced epitope retrieval was performed at 110 °C for 12 min with citrate buffer (pH 6.0). Anti-CD31/PECAM1 (1:100; Novus Biologicals, NB100-2284, Oakville, ON, Canada) primary antibodies were incubated for an hour at room temperature. The blocking reagent (Background Sniper, Biocare, Medical, Concord, CA, United States) and the MACH 4 detection system (Biocare Medical) were used according to manufacturer specifications. A Zeiss MIRAX MIDI Slide Scanner (Zeiss, Toronto, Canada) with 40× objective was used to image slices for cell infiltration, extracellular matrix deposition, and vascularization (angiogenesis). The micrographs were analyzed with the Panoramic Viewer (3DHISTECH Ltd., Budapest, Hungary) software.

Statistical Analysis. To assess statistical differences between the cells cultured on the biomaterials under the different conditions, one way ANOVA tests were used. The Tukey post hoc analysis was performed to determine the statistical difference between the individual samples. For the comparison of more than two samples, the one way ANOVA was used instead of multiple Student's *t* tests to reduce the risk of type I statistical errors. When only two samples were compared, the Student's *t* test was used. All values presented are the mean ± SEM. When dealing with biological samples, it is not possible to study the whole population; the standard error of the mean was used instead of the standard deviation because a representative sample is used as an estimate for the population. Statistical significance (indicated by an asterisk) refers to *P* < 0.05.

■ ASSOCIATED CONTENT

● Supporting Information

The Supporting Information is available free of charge on the ACS Publications website at DOI: 10.1021/acsbomaterials.8b00178.

Viable cell density chart, photo of cultured cells, Young's modulus measurements, and cell invasion and proliferation quantification (PDF)

■ AUTHOR INFORMATION

Corresponding Author

*Tel.: +1 613 562 5800 Ext. 6965; Fax: +1 613 562 5190; E-mail: a@pellinglab.net.

ORCID

Andrew E. Pelling: 0000-0003-3732-7472

Notes

The authors declare no competing financial interest.

■ ACKNOWLEDGMENTS

This work was supported by a Natural Sciences and Engineering Research Council (NSERC) Discovery Grant. R.J.H. was supported by an NSERC postgraduate scholarship and an Ontario Graduate Scholarship (OGS). D.J.M. was supported by a graduate student fellowship from the "Fonds de Recherche du Québec – Santé" (FRQS). A.E.P. gratefully acknowledges generous support from the Canada Research Chairs (CRC) program.

■ REFERENCES

- (1) Wang, H.; van Blitterswijk, C. A. The role of three-dimensional polymeric scaffold configuration on the uniformity of connective tissue formation by adipose stromal cells. *Biomaterials* **2010**, *31* (15), 4322–4329.
- (2) Syedain, Z.; Reimer, J.; Lahti, M.; Berry, J.; Johnson, S.; Tranquillo, R. T. Tissue engineering of acellular vascular grafts capable of somatic growth in young lambs. *Nat. Commun.* **2016**, *7*, 12951.
- (3) Wan, S.; Borland, S.; Richardson, S. M.; Merry, C. L. R.; Saiani, A.; Gough, J. E. Self-assembling peptide hydrogel for intervertebral disc tissue engineering. *Acta Biomater.* **2016**, *46*, 29.
- (4) Petrosyan, A.; Da Sacco, S.; Tripuraneni, N.; Kreuser, U.; Lavarreda-Pearce, M.; Tamburrini, R.; De Filippo, R. E.; Orlando, G.; Cravedi, P.; Perin, L. A step towards clinical application of acellular matrix: A clue from macrophage polarization. *Matrix Biol.* **2017**, *57–58*, 334.
- (5) Madl, C. M.; Katz, L. M.; Heilshorn, S. C. Bio-Orthogonally Crosslinked, Engineered Protein Hydrogels with Tunable Mechanics and Biochemistry for Cell Encapsulation. *Adv. Funct. Mater.* **2016**, *26*, 3612–3620.
- (6) Sánchez, P. L.; Fernández-Santos, M. E.; Costanza, S.; Climent, A. M.; Moscoso, I.; Gonzalez-Nicolas, M. A.; Sanz-Ruiz, R.; Rodríguez, H.; Kren, S. M.; Garrido, G.; et al. Acellular human heart matrix: A critical step toward whole heart grafts. *Biomaterials* **2015**, *61*, 279–289.
- (7) Khorramirouz, R.; Sabetkish, S.; Akbarzadeh, A.; Muhammadnejad, A.; Heidari, R.; Kajbafzadeh, A. M. Effect of three decellularisation protocols on the mechanical behaviour and structural properties of sheep aortic valve conduits. *Adv. Med. Sci.* **2014**, *59* (2), 299–307.
- (8) Gilbert, T. W.; Sellaro, T. L.; Badylak, S. F. Decellularization of tissues and organs. *Biomaterials* **2006**, *27* (19), 3675–3683.
- (9) Wang, Q.; Yang, H.; Bai, A.; Jiang, W.; Li, X.; Wang, X.; Mao, Y.; Lu, C.; Qian, R.; Guo, F.; et al. Functional engineered human cardiac patches prepared from nature's platform improve heart function after acute myocardial infarction. *Biomaterials* **2016**, *105*, 52–65.
- (10) de Oliveira Barud, H. G.; da Silva, R. R.; da Silva Barud, H.; Tercjak, A.; Gutierrez, J.; Lustri, W. R.; de Oliveira, O. B.; Ribeiro, S. J. L. A multipurpose natural and renewable polymer in medical applications: Bacterial cellulose. *Carbohydr. Polym.* **2016**, *153*, 406–420.
- (11) de Oliveira, G. M.; Basmaji, P.; Costa, L. M. M.; dos Santos, M. L.; dos Santos Riccardi, C.; Guastaldi, F. P. S.; Scarel-Caminaga, R. M.; de Oliveira Capote, T. S.; Pizoni, E.; Guastaldi, A. C. Surface physical chemistry properties in coated bacterial cellulose membranes with calcium phosphate. *Mater. Sci. Eng., C* **2017**, *75*, 1359–1365.
- (12) Jin, L.; Zeng, Z.; Kuddannaya, S.; Wu, D.; Zhang, Y.; Wang, Z. Biocompatible, Free-Standing Film Composed of Bacterial Cellulose

Nanofibers-Graphene Composite. *ACS Appl. Mater. Interfaces* **2016**, *8* (1), 1011–1018.

(13) Huang, J. W.; Lv, X. G.; Li, Z.; Song, L. J.; Feng, C.; Xie, M. K.; Li, C.; Li, H. B.; Wang, J. H.; Zhu, W. D.; et al. Urethral reconstruction with a 3D porous bacterial cellulose scaffold seeded with lingual keratinocytes in a rabbit model. *Biomed Mater.* **2015**, *10* (5), 55005.

(14) Galateanu, B.; Bunea, M.; Stanescu, P.; Vasile, E.; Casarica, A.; Iovu, H.; Hermenean, A.; Zaharia, C.; Costache, M. In Vitro Studies of Bacterial Cellulose and Magnetic Nanoparticles Smart Nanocomposites for Efficient Chronic Wounds Healing. *Stem Cells Int.* **2015**, *2015*, 1–10.

(15) Varma, D. M.; Gold, G. T.; Taub, P. J.; Nicoll, S. B. Injectable carboxymethylcellulose hydrogels for soft tissue filler applications. *Acta Biomater.* **2014**, *10* (12), 4996–5004.

(16) Unnithan, A. R.; Gnanasekaran, G.; Sathishkumar, Y.; Lee, Y. S.; Kim, C. S. Electrospon antibacterial polyurethane-cellulose acetate-zinc composite mats for wound dressing. *Carbohydr. Polym.* **2014**, *102* (1), 884–892.

(17) Pandit, V.; Zuidema, J. M.; Venuto, K. N.; Macione, J.; Dai, G.; Gilbert, R. J.; Kotha, S. P. Evaluation of multifunctional polysaccharide hydrogels with varying stiffness for bone tissue engineering. *Tissue Eng., Part A* **2013**, *19* (21–22), 2452–2463.

(18) Nimeskern, L.; Martínez Ávila, H.; Sundberg, J.; Gatenholm, P.; Müller, R.; Stok, K. S. Mechanical evaluation of bacterial nanocellulose as an implant material for ear cartilage replacement. *J. Mech. Behav. Biomed. Mater.* **2013**, *22*, 12–21.

(19) Pértile, R.; Moreira, S.; Andrade, F.; Domingues, L.; Gama, M. Bacterial cellulose modified using recombinant proteins to improve neuronal and mesenchymal cell adhesion. *Biotechnol. Prog.* **2012**, *28* (2), 526–532.

(20) Fang, B.; Wan, Y.-Z.; Tang, T.-T.; Gao, C.; Dai, K.-R. Proliferation and Osteoblastic Differentiation of Human Bone Marrow Stromal Cells on Hydroxyapatite/Bacterial Cellulose Nanocomposite Scaffolds. *Tissue Eng., Part A* **2009**, *15* (5), 1091–1098.

(21) Bodin, A.; Ahrenstedt, L.; Fink, H.; Brumer, H.; Risberg, B.; Gatenholm, P. Modification of nanocellulose with a xyloglucan-RGD conjugate enhances adhesion and proliferation of endothelial cells: Implications for tissue engineering. *Biomacromolecules* **2007**, *8* (12), 3697–3704.

(22) Helenius, G.; Bäckdahl, H.; Bodin, A.; Nannmark, U.; Gatenholm, P.; Risberg, B. In vivo biocompatibility of bacterial cellulose. *J. Biomed. Mater. Res., Part A* **2006**, *76* (2), 431–438.

(23) Svensson, A.; Nicklasson, E.; Harrah, T.; Panilaitis, B.; Kaplan, D. L.; Brittberg, M.; Gatenholm, P. Bacterial cellulose as a potential scaffold for tissue engineering of cartilage. *Biomaterials* **2005**, *26* (4), 419–431.

(24) Scherner, M.; Reutter, S.; Klemm, D.; Sterner-Kock, A.; Guschlbauer, M.; Richter, T.; Langebartels, G.; Madershahian, N.; Wahlers, T.; Wippermann, J. In vivo application of tissue-engineered blood vessels of bacterial cellulose as small arterial substitutes: Proof of concept? *J. Surg. Res.* **2014**, *189* (2), 340–347.

(25) Lee, C. M.; Kafle, K.; Park, Y. B.; Kim, S. H. Probing crystal structure and mesoscale assembly of cellulose microfibrils in plant cell walls, tunicate tests, and bacterial films using vibrational Sum Frequency Generation (SFG) spectroscopy. *Phys. Chem. Chem. Phys.* **2014**, *16* (22), 10844–10853.

(26) Barbié, C.; Chauveaux, D.; Barthe, X.; Baquey, C.; Poustis, J. Biological behavior of cellulosic materials after bone implantation: preliminary results. *Clin. Mater.* **1990**, *5* (2–4), 251–258.

(27) Miyamoto, T.; Takahashi, S. I.; Ito, H.; Inagaki, H.; Noishiki, Y. Tissue biocompatibility of cellulose and its derivatives. *J. Biomed. Mater. Res.* **1989**, *23* (1), 125–133.

(28) Martínez Ávila, H.; Feldmann, E. M.; Pleumeekers, M. M.; Nimeskern, L.; Kuo, W.; de Jong, W. C.; Schwarz, S.; Müller, R.; Hendriks, J.; Rotter, N.; et al. Novel bilayer bacterial nanocellulose scaffold supports neocartilage formation invitro and invivo. *Biomaterials* **2015**, *44*, 122–133.

(29) Wang, X.-Y.; Jin, Z.-H.; Gan, B.-W.; Lv, S.-W.; Xie, M.; Huang, W.-H.; et al. Engineering interconnected 3D vascular networks in

hydrogels using molded sodium alginate lattice as the sacrificial template. *Lab Chip* **2014**, *14* (15), 2709.

(30) Kirdponpattara, S.; Khamkeaw, A.; Sanchavanakit, N.; Pavasant, P.; Phisalaphong, M. Structural modification and characterization of bacterial cellulose-alginate composite scaffolds for tissue engineering. *Carbohydr. Polym.* **2015**, *132*, 146–155.

(31) Botton, S.; Robotti, F.; Jayathissa, P.; Hegglin, A.; Bahamonde, N.; Heredia-Guerrero, J. A.; Bayer, I. S.; Scarpellini, A.; Merker, H.; Lindenblatt, N.; et al. Surface-structured bacterial cellulose with guided assembly-based biolithography (GAB). *ACS Nano* **2015**, *9* (1), 206–219.

(32) Modulevsky, D. J.; Lefebvre, C.; Haase, K.; Al-Rekabi, Z.; Pelling, A. E. Apple derived cellulose scaffolds for 3D mammalian cell culture. *PLoS One* **2014**, *9* (5), e97835.

(33) Modulevsky, D. J.; Cuerrier, C. M.; Pelling, A. E. Biocompatibility of Subcutaneously Implanted Plant-Derived Cellulose Biomaterials. *PLoS One* **2016**, *11* (6), 1–19.

(34) Fontana, G.; Gershlak, J.; Adamski, M.; Lee, J.-S.; Matsumoto, S.; Le, H. D.; Binder, B.; Wirth, J.; Gaudette, G.; Murphy, W. L. Biofunctionalized Plants as Diverse Biomaterials for Human Cell Culture. *Adv. Healthcare Mater.* **2017**, *6*, 1601225.

(35) Gershlak, J.; Hernandez, S.; Fontana, G.; Perreault, L.; Hansen, K.; Larson, S.; Binder, B.; Dolivo, D.; Yang, T.; Dominko, T.; et al. Crossing kingdoms: Using decellularized plants as perfusable tissue engineering scaffolds. *Biomaterials* **2017**, *125*, 13–22.

(36) Zhu, W.; Zhao, Y.; Ma, Q.; Wang, Y.; Wu, Z.; Weng, X. 3D-printed porous titanium changed femoral head repair growth patterns: osteogenesis and vascularisation in porous titanium. *J. Mater. Sci.: Mater. Med.* **2017**, *28* (4), 62.

(37) Hinton, T. J.; Jallerat, Q.; Palchesko, R. N.; Park, J. H.; Grodzicki, M. S.; Shue, H.-J.; Ramadan, M. H.; Hudson, A. R.; Feinberg, A. W. Three-dimensional printing of complex biological structures by freeform reversible embedding of suspended hydrogels. *Sci. Adv.* **2015**, *1* (9), e1500758–e1500758.

(38) Sammalkorpi, M.; Karttunen, M.; Haataja, M. Ionic surfactant aggregates in saline solutions: Sodium dodecyl sulfate (SDS) in the presence of excess sodium chloride (NaCl) or calcium chloride (CaCl₂). *J. Phys. Chem. B* **2009**, *113* (17), 5863–5870.

(39) Corrin, M. L.; Harkins, W. D. The effect of salts on the critical concentration for the formation of micelles in colloidal electrolytes. *J. Am. Chem. Soc.* **1947**, *69* (3), 683–688.

(40) Yang, J.; Zhang, Y. S.; Yue, K.; Khademhosseini, A. Cell-Laden Hydrogels for Osteochondral and Cartilage Tissue Engineering. *Acta Biomater.* **2017**, *57*, 1.

(41) Sugibayashi, K.; Kumashiro, Y.; Shimizu, T.; Kobayashi, J.; Okano, T. A molded hyaluronic acid gel as a micro-template for blood capillaries. *J. Biomater. Sci., Polym. Ed.* **2012**, *24* (2), 135–147.

(42) Ninan, G.; Joseph, J.; Aliyamveetil, Z. A. A comparative study on the physical, chemical and functional properties of carp skin and mammalian gelatins. *J. Food Sci. Technol.* **2014**, *51* (9), 2085–2091.

(43) Chaturvedi, V.; Dye, D. E.; Kinnear, B. F.; Van Kuppevelt, T. H.; Grounds, M. D.; Coombe, D. R. Interactions between skeletal muscle myoblasts and their extracellular matrix revealed by a serum free culture system. *PLoS One* **2015**, *10* (6), 1–27.

(44) Al-Rekabi, Z.; Pelling, A. E. Cross talk between matrix elasticity and mechanical force regulates myoblast traction dynamics. *Phys. Biol.* **2013**, *10* (6), 66003.

(45) Engler, A. J.; Griffin, M. a.; Sen, S.; Bönnemann, C. G.; Sweeney, H. L.; Discher, D. E. Myotubes differentiate optimally on substrates with tissue-like stiffness: pathological implications for soft or stiff microenvironments. *J. Cell Biol.* **2004**, *166* (6), 877–887.

(46) Ravi, M.; Paramesh, V.; Kaviya, S. R.; Anuradha, E.; Paul Solomon, F. D. 3D cell culture systems: Advantages and applications. *J. Cell. Physiol.* **2015**, *230* (1), 16–26.

(47) Knight, E.; Przyborski, S. Advances in 3D cell culture technologies enabling tissue-like structures to be created in vitro. *J. Anat.* **2015**, *227* (6), 746–756.

(48) Qin, X.; Riegler, J.; Tiburcy, M.; Zhao, X.; Chour, T.; Ndoye, B.; Nguyen, M.; Adams, J.; Ameen, M.; Denney, T. S.; et al. Magnetic

Resonance Imaging of Cardiac Strain Pattern Following Transplantation of Human Tissue Engineered Heart Muscles. *Circ. Cardiovasc. Imaging* **2016**, *9* (11), e004731.

(49) Sun, H.; Zhou, J.; Huang, Z.; Qu, L.; Lin, N.; Liang, C.; Dai, R.; Tang, L.; Tian, F. Carbon nanotube-incorporated collagen hydrogels improve cell alignment and the performance of cardiac constructs. *Int. J. Nanomed.* **2017**, *12*, 3109–3120.

(50) Paleologos, E. K.; Giokas, D. L.; Karayannis, M. I. Micelle-mediated separation and cloud-point extraction. *TrAC, Trends Anal. Chem.* **2005**, *24* (5), 426–436.

(51) Park, J. H.; Jung, J. W.; Kang, H.-W.; Cho, D.-W. Indirect three-dimensional printing of synthetic polymer scaffold based on thermal molding process. *Biofabrication* **2014**, *6* (2), 25003.

(52) Käpylä, E.; Delgado, S. M.; Kasko, A. M. Shape-Changing Photodegradable Hydrogels for Dynamic 3D Cell Culture. *ACS Appl. Mater. Interfaces* **2016**, *8* (28), 17885–17893.

(53) Hendriks, J.; Riesle, J.; van Blitterswijk, C. A. Co-culture in cartilage tissue engineering. *J. Tissue Eng. Regen. Med.* **2007**, *1* (3), 170.

(54) Sender, R.; Fuchs, S.; Milo, R. Revised Estimates for the Number of Human and Bacteria Cells in the Body. *PLoS Biol.* **2016**, *14* (8), 1–14.

(55) Feng, B.; Jinkang, Z.; Zhen, W.; Jianxi, L.; Jiang, C.; Jian, L.; Guolin, M.; Xin, D. The effect of pore size on tissue ingrowth and neovascularization in porous bioceramics of controlled architecture in vivo. *Biomed. Mater.* **2011**, *6* (1), 15007.

(56) Sandiford, N.; Doctor, C.; Rajaratnam, S. S.; Ahmed, S.; East, D. J.; Miles, K.; Butler-Manuel, A.; Shepperd, J. A. N. Primary total hip replacement with a Furlong fully hydroxyapatite-coated titanium alloy femoral component: Results at a minimum follow-up of 20 years. *Bone Jt. J.* **2013**, *95-B* (4), 467–471.

(57) Van Nooten, G. J.; Bové, T.; Van Belleghem, Y.; François, K.; Caes, F.; Vandenplas, G.; De Pauw, M.; Taeymans, Y. Twenty-year single-center experience with the medtronic open pivot mechanical heart valve. *Ann. Thorac. Surg.* **2014**, *97* (4), 1306–1313.

(58) Truernit, E.; Bauby, H.; Dubreucq, B.; Grandjean, O.; Runions, J.; Barthelemy, J.; Palauqui, J. C. High-resolution whole-mount imaging of three-dimensional tissue organization and gene expression enables the study of Phloem development and structure in *Arabidopsis*. *Plant Cell* **2008**, *20* (6), 1494–1503.